The Mass, Absolute Angular Momentum and Kinetic Energy Budgets of Model-Generated Extratropical Cyclones and Anticyclones

WILLIAM K. DOWNEY

Australian Numerical Meteorology Research Centre, Melbourne, Australia

DONALD R. JOHNSON

Department of Meteorology and Space and Engineering Center, University of Wisconsin, Madison 53706

(Manuscript received 1 December 1976, in final form 31 December 1977)

ABSTRACT

The budgets of mass, absolute angular momentum and kinetic energy for two model-generated cyclones and one anticyclone are examined using a sigma-coordinate framework which moves with the center of the MSL pressure extremum. The mass budgets for all three cases show a concentration of lateral mass transport in the surface boundary layer and at a level near 200 mb. The spin up of the low troposphere during cyclogenesis results from the dominance of the mean mode of lateral transport of absolute angular momentum. The spin up of the upper troposphere results from the combined influence of an inward eddy mode of lateral transport and vertical transport of absolute angular momentum. The eddy mode of lateral transport is determined by the configuration of the upper level flow (particularly jet streaks) and is enhanced by frontogenesis in the low and mid-troposphere as these regions spin up. The increase of kinetic energy in the low troposphere during cyclogenesis results from the dominance of local generation by cross-isobar flow toward the center of the developing vortex. In the upper troposphere the kinetic energy budget is not related uniquely to the development or decay of the surface cyclone. While the anticyclone, to a large extent, displays similar behavior to the cyclone, the eddy mode of lateral transport of angular momentum in the upper troposphere is not enhanced by lower level frontogenetic effects, as in the case of the cyclone.

1. Introduction

Cyclogenesis[1] might best be described as a system in which there is a decrease of mass, an increase of kinetic energy (at least in the lower troposphere), and a concentration of angular momentum about a local axis. As noted by Starr (1953), a fundamental problem of meteorology may be formulated by asking how the rise and fall in these properties can be accounted for within a prescribed region of space. A diagnostic framework which can be utilized to examine some of these aspects is outlined in Johnson and Downey (1975a). The method involves placing a conical shell around the cyclone (the central axis of the cone being coincident with and moving with the surface pressure minimum), and examining the budgets of fundamental quantities such as mass, kinetic energy and angular momentum within this moving volume. This affords a perspective on the interaction of the synoptic scale with its environment. The physical principles of interaction are quantified through the transport relations and other governing equations. The formulation enables one to study the exchange of properties through the prescribed boundaries while sources/sinks of these properties are identified with physical and dynamical processes within the volume. By such diagnostic examinations of cyclogenesis in both numerical models and the real atmosphere, one would hope to gain further insight into the physical and dynamical processes involved. Where model cyclogenesis compares favorably with the real atmosphere, the model with its internally consistent data base may well provide more insight into the mass, angular momentum and energy adjustments that occur during cyclogenesis. Where the models diverge from the real atmosphere, the diagnostics of the latter may isolate the reasons. In this paper we consider cases of model cyclogenesis and anticyclogenesis and attempt to examine some of the problems which prove to be extremely elusive in the real atmosphere because of the inherent difficulties of measurement on the required time and space scales; e.g., what is the relevance of kinetic energy transport versus local generation in the energetic maintenance of the vortex?; by what means does the local buildup of angular momentum occur?; and what leads to the vertical collinearity of the system that typifies the "occlusion phase" of the cyclone?

[1] The predominant reference to the cyclone in general discussions throughout this paper is not intended to detract from the importance of the anticyclone but simply avoids continual contradistinction between the two.

2. The Equations

The coordinate system used (Fig. 1) is a Southern Hemisphere counterpart of Johnson and Downey

0027-0644/78/0469-0481$06.50

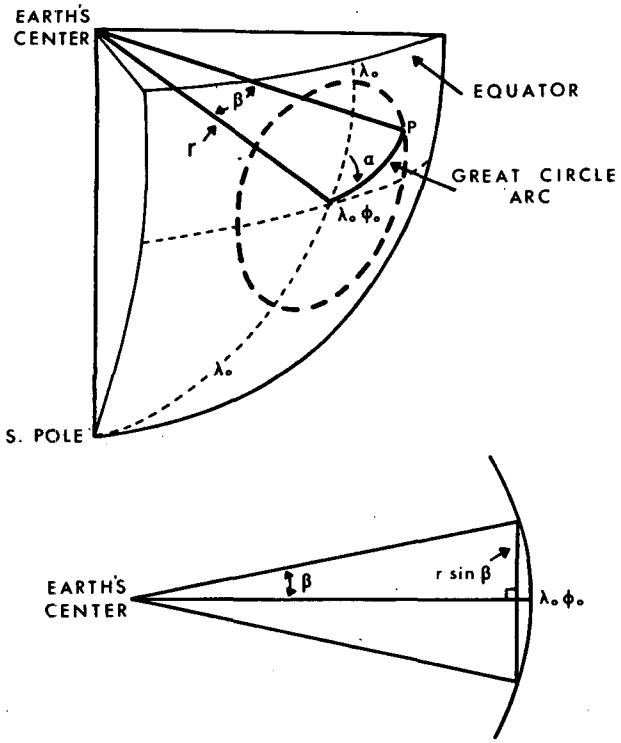

FIG. 1. The coordinate system illustrating (i) the center of the budget volume (λ_0, ϕ_0); (ii) the lateral boundary of the budget volume (heavy dashed line), defined by the angle β; and (iii) an arbitrary point P referenced by the coordinates α, β.

(1975a). The budget equation in sigma coordinates is given by

$$\frac{dF}{dt}=\int_0^1\int_0^{\beta_B}\int_0^{2\pi}\frac{p_*}{g}\frac{df}{dt}r^2\sin\beta d\alpha d\beta d\sigma - \int_0^1\int_0^{2\pi}\frac{p_*}{g}f(U-W)_\beta r\sin\beta d\alpha d\sigma\Big|_{\beta_B} + \int_0^1\int_0^{\beta_B}\int_0^{2\pi}\frac{p_*}{g}\frac{\partial}{\partial\sigma}(f\dot{\sigma})r^2\sin\beta d\alpha d\beta d\sigma, \quad (1)$$

where

$$F=\int_0^1\int_0^{\beta_B}\int_0^{2\pi}\frac{p_*}{g}fr^2\sin\beta d\alpha d\beta d\sigma \quad (2)$$

and f is an arbitrary budget quantity (e.g., angular momentum, moisture, energy per unit mass). See Appendix A for a list of symbols.

Note that the last term in Eq. (1) is, in fact, zero since there can be no transport through the earth's surface or the top of the atmosphere. The term is included to indicate the form of the vertical transport term when the limits of integration are not $\sigma=0$ and $\sigma=1$:

For the mass budget

$$f=1;\quad \frac{df}{dt}=0. \quad (3)$$

For the kinetic energy budget

$$f=\tfrac{1}{2}(U_\alpha^2+U_\beta^2), \quad (4)$$

$$\frac{df}{dt}=\mathbf{U}\cdot\left[\nabla_\sigma\Phi+\frac{RT}{p_*}\nabla_\sigma p_*\right]+\mathbf{U}\cdot\mathbf{F}. \quad (5)$$

[See Smagorinsky *et al.* (1965) for the detailed "model" formulation of the friction force **F**.]

For the absolute angular momentum budget

$$f=g_a=\left[\tfrac{1}{2}\Omega(\sin\phi+\sin\phi_0)+\frac{(U-W)_\alpha}{r\sin\beta}\right]r^2\sin^2\beta, \quad (6)$$

$$\frac{df}{dt}=\underbrace{\frac{\partial\phi}{\partial\alpha}+\frac{RT}{p_*}\frac{\partial p_*}{\partial\alpha}}_{\text{Pressure torque}}+\underbrace{F_\alpha r\sin\beta}_{\text{Frictional torque}}+\underbrace{I_T}_{\text{Inertial torques}}. \quad (7)$$

The form of the absolute angular momentum in Eq. (6) is more general than that used in Johnson and Downey (1975b).

Subsequent to the formulation of absolute angular momentum of storms, an expression that includes the effects of the earth's sphericity in the definition of the earth component of angular momentum and an additional term for the tendency of the vector property have been derived. The approximation for the earth component in (6) that is useful with storm volumes of limited horizontal extent (valid to 3% if β is equal to or less than 12°, radius $\approx$1300 km) has been utilized. The additional term for the tendency of the vector property is an inertial effect and stems from the rotation of the quasi-Lagrangian coordinate system due to its translation over a curved earth surface. Within the storm coordinate system, the effect is to rotate the angular momentum of the storm and provide for a redistribution of the vector property among its components without ever changing the magnitude of the vector property. In theory, the component of angular momentum along the storm's axis of rotation has potential sources from angular momentum components about two horizontal axes of rotation. Diagnostic results to date substantiate that this effect is minimal due to the condition that the angular momentum components about horizontal axes are small. For the model storms the pressure and inertial torques evaluated in sigma coordinates were generally found to be one to two orders of magnitude smaller than the other budget terms. A reasonable approximation for (7) is

$$\frac{df}{dt}\approx F_\alpha r\sin\beta. \quad (8)$$

MEAN AND EDDY MODES OF LATERAL TRANSPORT

Following Johnson and Downey (1975a) the lateral transport may be decomposed into a mean and eddy

mode given by

$$\int_0^1\int_0^{2\pi}\frac{p_*}{g}f(U-W)_\beta r\sin\beta d\alpha d\sigma$$

$$=\int_0^1\int_0^{2\pi}\frac{\overline{p_*}^\alpha}{g}\langle f\rangle^\alpha\langle(U-W)_\beta\rangle^\alpha r\sin\beta d\alpha d\sigma \quad \text{(Mean mode)}$$

$$+\int_0^1\int_0^{2\pi}\frac{\overline{p_*}^\alpha}{g}\langle f^*(U-W)^*_\beta\rangle^\alpha r\sin\beta d\alpha d\sigma, \quad (9)$$

(Eddy mode)

where the averaging operators and departures are defined for an arbitrary quantity Q by

$$\overline{Q}^\alpha=\int_0^{2\pi}Qd\alpha, \quad Q=\overline{Q}^\alpha+Q', \tag{10}$$

$$\langle Q\rangle^\alpha=\overline{p_*Q}^\alpha/\overline{p_*}^\alpha, \quad Q=\langle Q\rangle^\alpha+Q^*. \tag{11}$$

3. The model

The model used in this work is a Southern Hemisphere version of the 9-level primitive equation stereographic model developed at the Geophysical Fluid Dynamics Laboratory, Princeton (Smagorinsky *et al.*, 1965; Manabe *et al.*, 1965). A polar stereographic projection of the hemisphere is covered by a 61×61 square grid

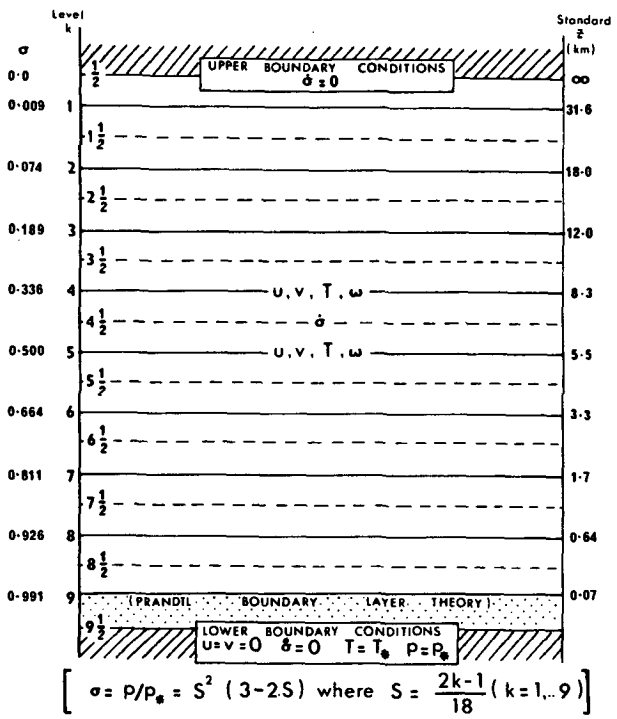

FIG. 2. The vertical structure, boundary conditions and variables carried in the 9-level stereographic model.

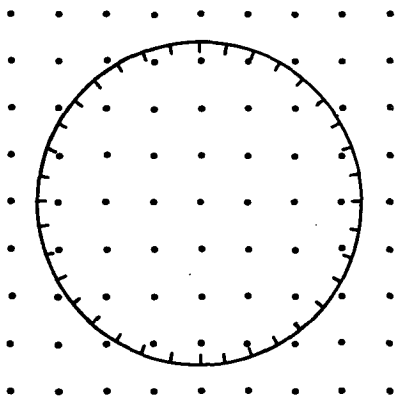

FIG. 3. Points on the square grid in relation to the 36 points on the lateral boundary of a budget volume of radius 10° latitude. Note that the actual boundary is more elliptic (see text), but for simplicity is depicted here as a circle. For the purpose of area averaging four additional internal rings (2° latitude increments) are used.

(i.e., 30 points between pole and equator). This gives a horizontal resolution of ~400 km in middle latitudes. A hydrologic cycle is included. The vertical distribution of levels, boundary conditions and variables carried in the model are indicated in Fig. 2. Other features of the Southern Hemisphere version are summarized in Appendix B.

The prediction of the secondary scale by the model suffers from the following three limitations:

1) Insufficient vertical resolution (and possibly physics) to adequately capture the tropopause structure and the jet stream

2) Limited boundary layer physics which affects the surface heat and moisture exchanges

3) Simple convective adjustment of the lapse rates of temperature and moisture.

However, despite these limitations, cyclones and anticyclones are generated in the model in realistic geographical locations and do appear to have many of the characteristics which are noted in their real atmosphere counterparts (Anderson and Noar, 1974; Simpson and Downey, 1975).

4. Data processing

In the normal model configuration data are available on the square grid mentioned in Section 3. After establishing the center of the budget volume a series of 36 points (Fig. 3) are established along a number of concentric equidistant "quasi-circular" rings on the stereographic projection[2]; e.g., for a budget volume defined by an outer radius of 10° latitude, five radii are used at intervals of 2° latitude. The field quantities

[2] Because a stereographic projection is involved, the surface of intersection of a cone from the earth's center and the earth's surface appears as a distorted circle.

used in the budget study (u, v, ϕ, etc.) are then interpolated to the 36 points on the various rings. The interpolation scheme involves a simple inverse square distance weighting procedure. With the raw data interpolated to the concentric arrays, the wind components are resolved into tangential (U_α) and radial (U_β) components. The radial component is required for the lateral transport term and the tangential component in the angular momentum formulation. **W** is diagnosed from successive positions of the surface pressure minimum. The kinetic energy generation term and the dissipation term are computed on the stereographic grid and then interpolated to the concentric grid. Line averages are achieved by summation around the 36 points of the lateral boundary. Area averages are achieved by summation of appropriately area weighted line averages for the equidistant rings.

5. Case Studies

Two cases of cyclogenesis and one of anticyclogenesis are examined.

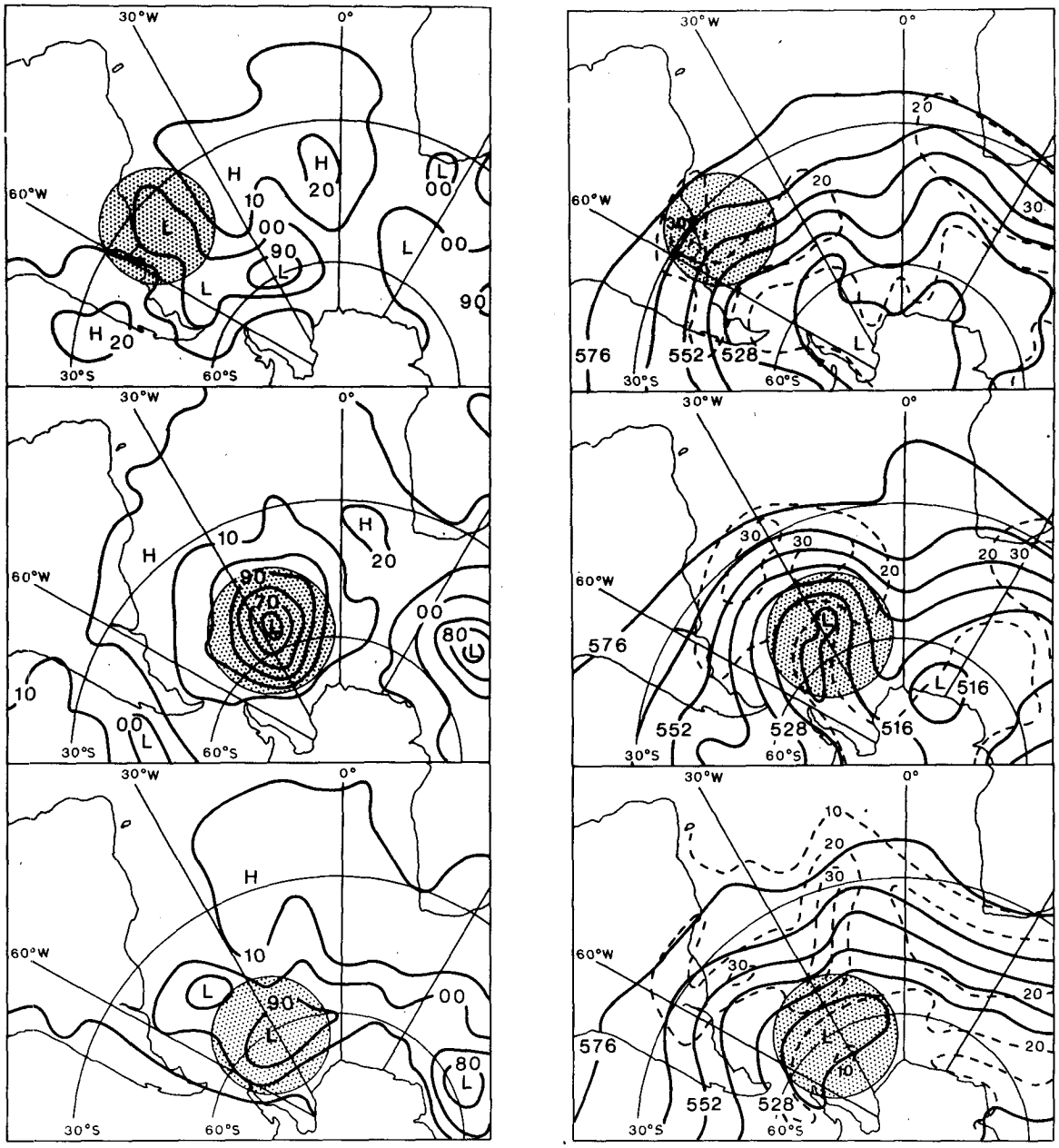

FIG. 4. Broadscale features of (a) mean sea level pressure (mb) and (b) 500 mb geopotential height (geopotential decameters) and isotachs (dashed, m s^{-1}) for Day 1 (top), Day 4 (middle), Day 7 (bottom). (Hatching denotes the budget area of radius 12° latitude).[4]

a. Cyclone 1 (C1)

This cyclone developed in the Argentine Basin around Day 75 of a long-term (100 day) model integration. (For convenience we will refer to the sequence of interest in terms of Day 1, Day 2, etc.) Fig. 4 shows a sequence of MSL and 500 mb charts depicting the development in a broadscale context.[3] The central MSL pressures falls are of order 40 mb, and much of this change occurs during the first two days. At 500 mb the initially weak trough just off the east coast of South America on Day 1 amplifies greatly and geopotential falls approaching 400 m are detected between Days 1 and 4. Note that on Day 4 the 500 mb trough extends from just west of the surface center to just north of it. By Day 7 the northern part of this trough appears to be moving away as a distinct short-wavelength feature while a new surface cyclone and 500 mb trough amplify in the Argentinian Basin. Fig. 5 summarizes the changes in the net mass, angular momentum and kinetic energy which attend the synoptic features just discussed. The total mass curve shows intense development over the first 2–3 days, near steady-state condition for 2–3 days, followed by rapid filling. The total absolute and relative angular momentum tendencies are large and positive for the first 2–3 days, then relatively steady for the next 4 days. The relative angular momentum decreases significantly in the final day. The total kinetic energy shows a general decline for the first 6 days, the largest decreases occurring between Days 2 and $4\frac{1}{2}$. There is a relatively weak and temporary increase of total kinetic energy around Day 7.

We now examine the role of the component terms of the various budgets in producing these observed tendencies and in particular their vertical distribution.

1) MASS BUDGET

Fig. 6a shows the vertical distribution of the lateral mass transport at selected intervals throughout the life cycle of the cyclone. In the early stages the lower half of the atmosphere is classically convergent and the upper half divergent (Bjerknes, 1937; Bjerknes and Holmboe, 1944). With time the upper divergent branch is lost and in the final stages reverts to being convergent. The surface boundary layer remains convergent throughout. Following the peak of surface development (around Day 4) the layer between $\sigma=0.5$ and the top of the boundary layer is systematically divergent. If the interpolation of fields from the square grid to the circular lateral boundary of the budget volume were free of error, then the integration of the mass transport profiles would correspond exactly with the pressure

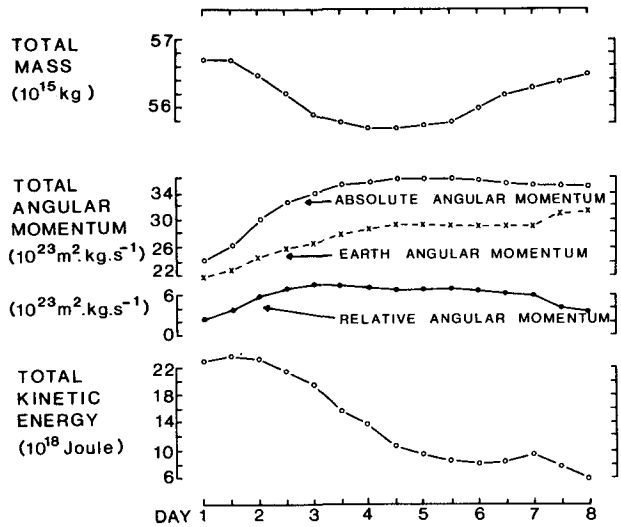

FIG. 5. Temporal distribution of the total mass, angular momentum and kinetic energy for cyclone C1.

tendency for the budget volume. The latter is proportional to the slope of the total mass curve in Fig. 5. In general there are errors introduced by the interpolation procedure and in estimating **W** and the desired accuracy is not achieved. By way of illustration a mass flux of 0.13×10^{10} kg s^{-1} is equivalent to an area-averaged pressure tendency of 3 mb day^{-1}. This could be produced by a mean inward/outward velocity throughout the atmosphere of 0.02 m s^{-1}. Alternatively, this would require that the total area under the curve in Fig. 7a (Day 1, say) be accurate to within 3%, whereas an optimistic estimate of the expected error is nearer 6%. Despite these accuracy limitations, the temporal and spatial continuity of the profiles leaves little doubt as to the layered structure of the mass circulation as previously described.

We now examine the way in which angular momentum and kinetic energy are transported and redistributed by this mass circulation as well as the way in which these properties are affected by friction.

2) THE ABSOLUTE ANGULAR MOMENTUM BUDGET

Before examining the vertical distribution of the budget terms (Fig. 6b), it is appropriate to first look at the total budget and the vertical distribution of angular momentum itself (Fig. 7). Since there are no net internal sources of absolute angular momentum, any net buildup must come from the excess of lateral transport (LT) over frictional torques (FT). Fig. 7a shows the temporal distribution of LT, FT and LT +FT. Because the net LT involves the small difference of large numbers of opposite signs, each of which is subject to the aforementioned interpolation errors and the subjective procedure of establishing the center of rotation (and thereby **W**), it is necessary to apply a least-squares fit to LT. When this is done the form of

[3] The stippled areas in Fig. 4 are those used in the budget calculations and are defined by a radius of 12° latitude.

[4] This radius was subjectively deemed to incorporate most of the surface cyclone at maturity. For the smaller and weaker cyclone (C2) a radius of 10° latitude was similarly selected.

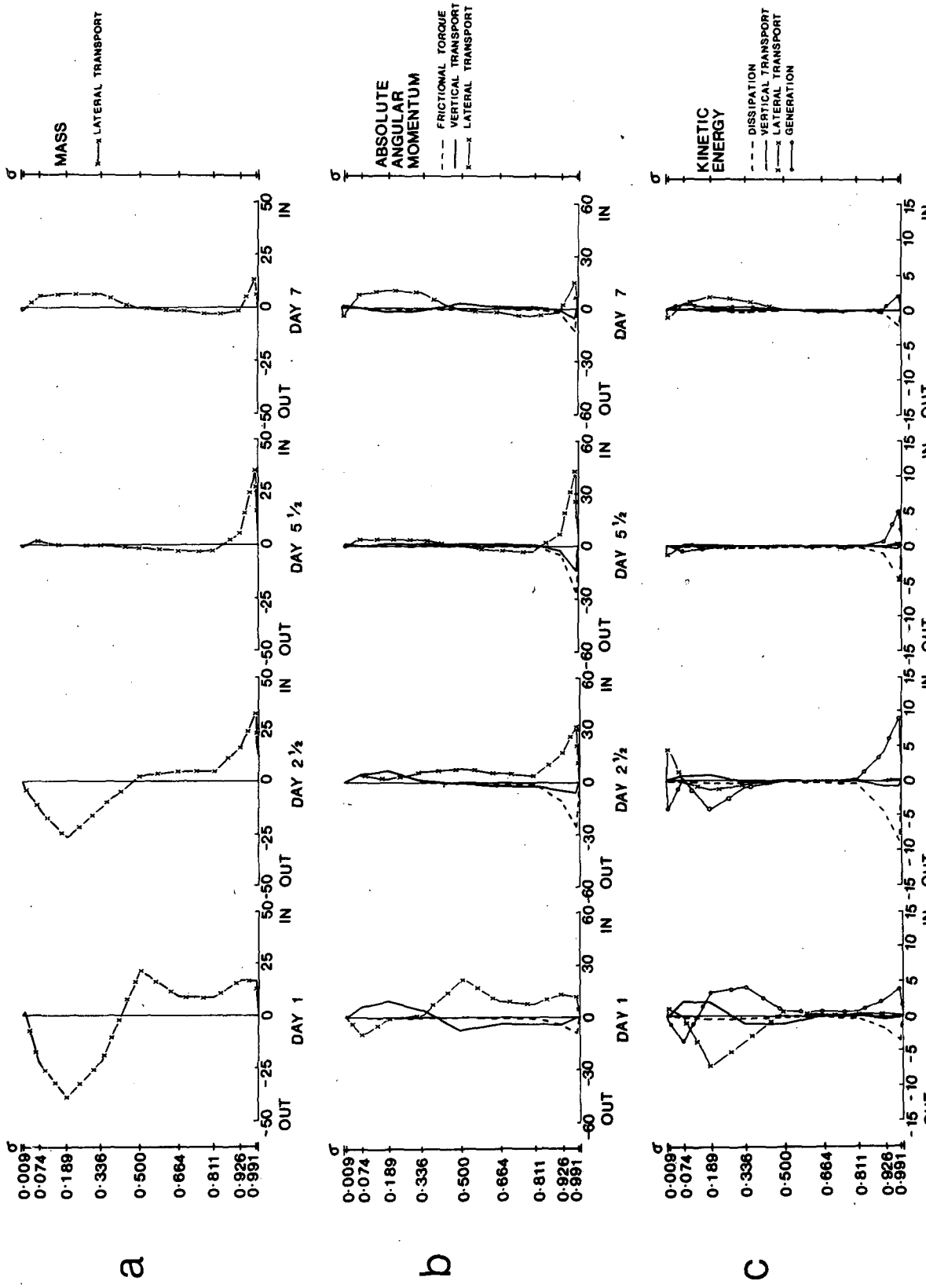

FIG. 6. Vertical profiles of (a) the lateral mass transport (10^{10} kg s^{-1} atm^{-1}); (b) the component terms of the absolute angular momentum budget (10^{18} m^2 kg s^{-2} atm^{-1}); (c) the component terms of the kinetic energy budget (10^{14} W atm^{-1}). The area of the budget volume defined by a radius of 12° latitude is $\sim 0.55 \times 10^{13}$ m^2.

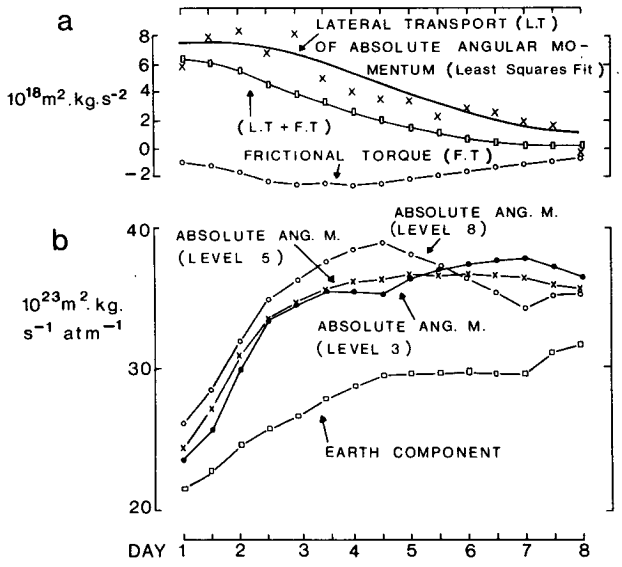

FIG. 7. Temporal distribution of (a) the component terms of the total absolute angular momentum budget and (b) the absolute angular momentum at level $8 \equiv \sigma = 0.926$, level $5 \equiv \sigma = 0.5$, level $3 \equiv \sigma = 0.189$. (The "earth component" of absolute angular momentum is also shown.)

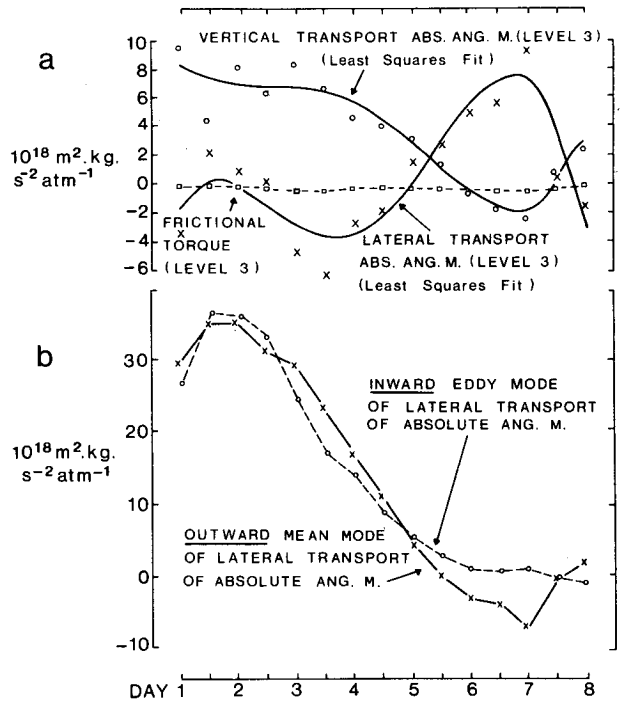

FIG. 8. Temporal distribution of (a) the component terms of the absolute angular momentum budget for level 3 ($\sigma = 0.189$) and (b) the mean and eddy modes of lateral transport of absolute angular momentum for level 3 ($\sigma = 0.189$).

the LT+FT curve is in good agreement with the observed tendency of absolute angular momentum. However, while the LT+FT curve remains positive throughout the entire 8-day period the observed tendency is weakly negative following Day 5. So far the reasons for this discrepancy have not been completely isolated, but an expected error analysis suggests that it is most likely due to interpolated deficiencies in the high-gradient regions of the jet stream, the transport term being most affected.

Fig. 7b shows two interesting interrelated features: 1) the vertical gradient of angular momentum reverses around Day $5\frac{1}{2}$; and 2) between Days $4\frac{1}{2}$ and 7 levels 8 and 3 exhibit reverse tendencies, i.e., the upper troposphere continues to spin up while the low troposphere spins down.

To examine these features more closely, we must look to the local budgets in the upper and lower troposphere. It is clear from Fig. 6b that the spin up of the low troposphere must result from the excess of the local lateral transport over frictional torques and upward vertical transport. In the upper troposphere the situation is more complex with both the vertical and horizontal transport playing an important role. Fig. 8a shows the relative contributions of these terms for level 3. Initially the vertical transport of angular momentum dominates, while in the latter days the lateral transport dominates and for a day or so the vertical transport reverts to being downward. Fig. 8b shows the relative roles of the mean and eddy modes of lateral transport [defined in Eq. (9)]. In agreement with the characteristics noted earlier with regard to the mass circulation, the mean mode of lateral transport of absolute angular momentum is large and outward during the earliest stages of development and reverts to inward in the latter stages. The eddy mode is continually inward, its magnitude increases briefly during the first day or so of development, then decreases

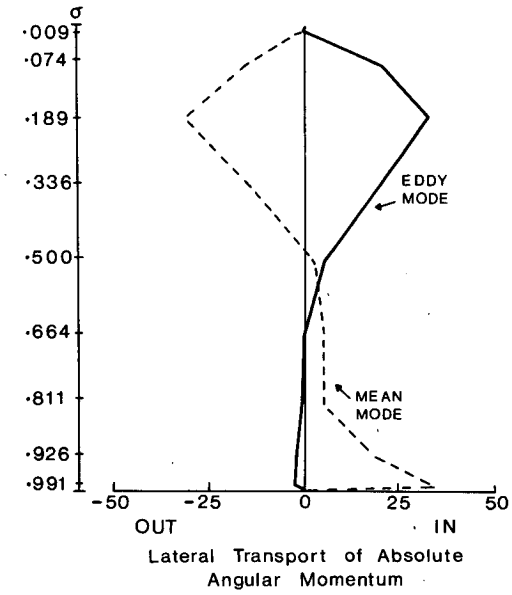

FIG. 9. Vertical profile of the mean and eddy modes of lateral transport of absolute angular momentum for Day $2\frac{1}{2}$ (10^{18} m^2 kg s^{-2} atm^{-1}).

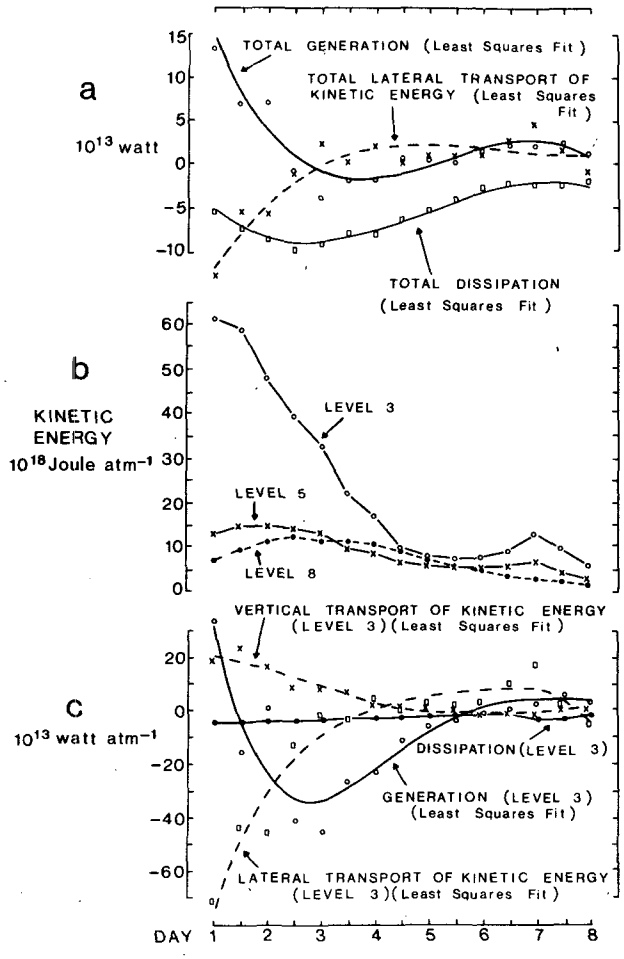

FIG. 10. Temporal distribution of (a) the component terms of the total kinetic energy budget, (b) the kinetic energy at three selected levels and (c) the component terms of the kinetic energy budget for level 3 ($\sigma=0.189$).

to near-zero values as the cyclone occludes and declines. The importance of this eddy mode in offsetting the mean mode has been stressed in earlier work (Johnson and Downey, 1975b, 1976) and results from the initial configuration of the upper level flow (particularly the jet stream) and the subsequent mutual adjustments to the rotational deformations of the lower and middle-level baroclinic zone which attend the low-level development. Contrastingly, as shown in Fig. 9, the mean mode of transport dominates in the low tropospheric buildup of angular momentum. An interesting feature in the latter stages of the life cycle (Days 6–7, Fig. 8b) is the substantial inward transport by the mean mode in the upper levels as the mass circulation there reverts to being inward. The now cooperative influence of the mean and eddy mode enable the upper regions to spin up substantially, while the lower troposphere spins down. As noted earlier, we do, however, overestimate the transport since Fig. 8a indicates an excess of inward LT into Day $7\frac{1}{2}$, whereas the observed absolute angular momentum tendency at level 3 (Fig. 7b) is distinctly negative following Day 7.

3) The kinetic energy budget

As noted, the total kinetic energy exhibits a general decrease with time. Fig. 11a shows the component terms of the total kinetic energy budget. The early stages are characterized by large positive generation and lateral export of kinetic energy. With time both the total generation and lateral transport are reduced substantially from the initially large values. The total generation reverts to being negative between Days 3 and 5 and positive again between Days 6 and 8. The lateral transport of kinetic energy reverts to an inward component around Day 3 and remains so thereafter. The dissipation peaks at around Day $2\frac{1}{2}$, whereas one might have expected it to follow the total mass transport profile more closely and peak around Day 4. Fig. 10b shows that the main contribution to the tendency of the total kinetic energy resides with the tendency in the upper levels where most of the kinetic energy is initially concentrated. Fig. 10c portrays the component budget terms for level 3. The notable characteristics are as follows:

(i) Initially large positive generation (Day 1) reverts to large negative generation by Day $2\frac{1}{2}$ then gradually increases back to near-zero values by Day $5\frac{1}{2}$.

(ii) The vertical transport of kinetic energy decreases monotonically from initially large positive values to near zero values by Day $5\frac{1}{2}$.

(iii) The lateral transport of kinetic energy is initially large and outward, reverts to being inward around Day 4, with a comparatively weak maximum around Day 7.

(iv) Dissipation is relatively weak and remains fairly constant throughout.

This conveys a relatively complex interplay of the component terms in the upper levels. In contrast, Fig. 6c shows the kinetic energy budget of the lower troposphere to be quite systematic. The buildup (decline) results from the excess (deficit) of local generation over dissipation and vertical transport.

b. Cyclone 2 (C2)

Whereas C1 is a case of intense surface cyclogenesis, C2 is relatively weak and does not exhibit the extreme convolution of the upper flow noted in C1 and in strongly occluded cyclones in the real atmosphere. It is therefore of some interest to examine the budgets of C2 and look for invariant and variant features between C1 and C2.

Fig. 11 shows the broadscale MSL pressure and 500 mb geopotential height for Days 1, 4 and 8. It is most noticeable that the 500 mb pattern suggests the upper levels retain the character of an open wave

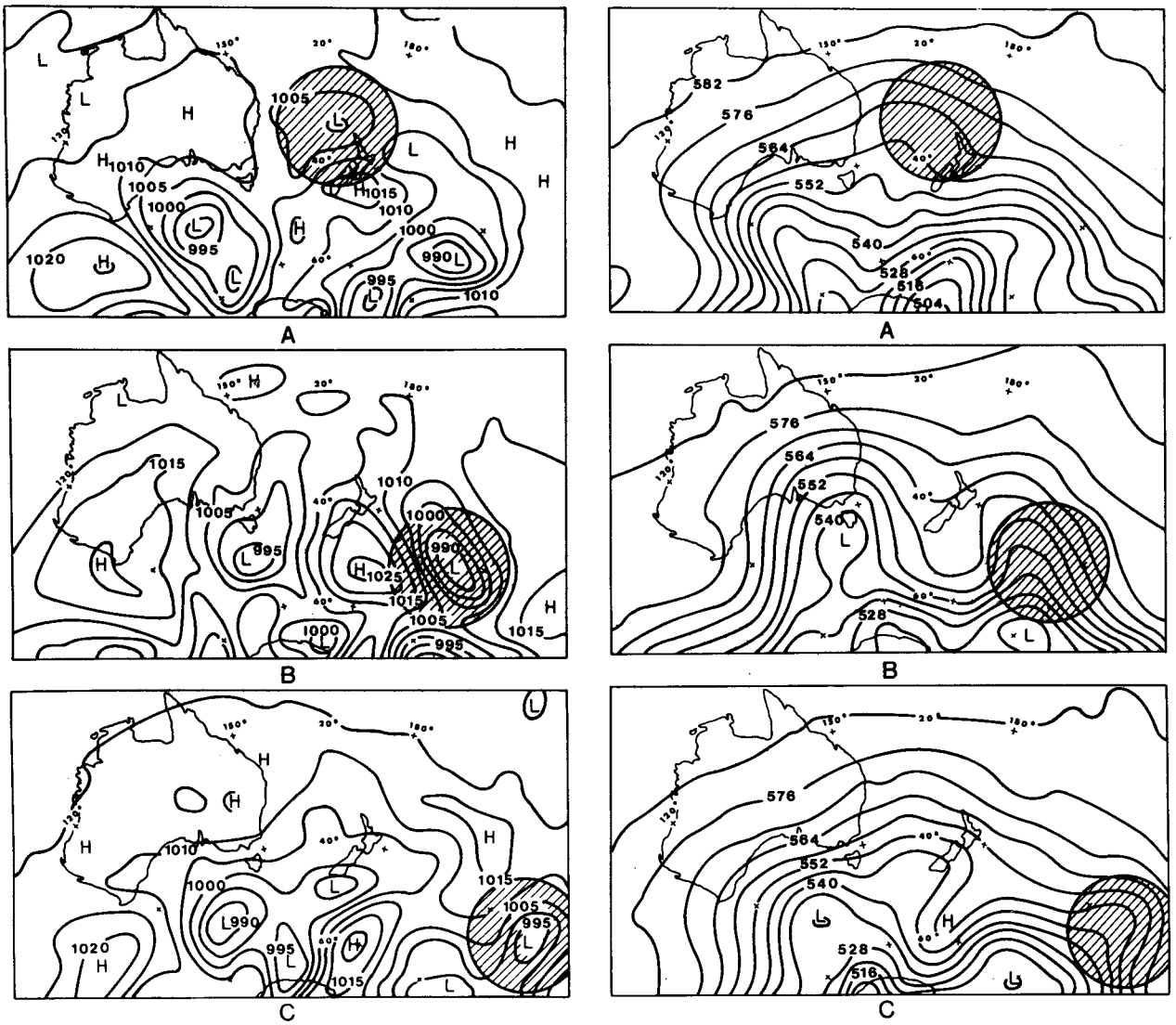

FIG. 11. Broadscale features of (a) mean sea level pressure (mb) and (b) 500 mb geopotential height (geopotential decameters): Day 1 (top), Day 4 (middle), Day 8 (bottom). (Stippling denotes the budget area of radius 10° latitude for cyclone C2.)

throughout. Other features noted in a detailed examination of 12 h charts are as follows:

1) The MSL pressure distribution is particularly asymmetric between Days 3 and 7 and reflects the mutual adjustment of the mass and momentum fields to the propagating jet streak in the upper levels. (Note the NW–SE orientation of the MSL isotach maxima at 500 and 200 mb).

2) The isotach distributions at 200 mb (not shown) suggest a substantial change in the kinetic energy between the early stages of development when a branch in the southeast quadrant dominates the volume, and the later stages when a branch in the northwest quadrant plays a role. An increase in angular momentum is also implied.

Fig. 12 shows the total mass, angular momentum and kinetic energy variations for a budget volume defined by a radius of 10° latitude (12° latitude was used for C1). The main difference from C1 is in the total kinetic energy signature. Here the total kinetic energy increases until Day 5 (the peak of surface development) and then decreases. We shall examine this aspect in more detail later.

The vertical profiles of the lateral mass transport for C2 showed the same characteristics as those for the early stages of C1 with a level of nondivergence around 500 mb. However, there was no complete reversal of the mass circulation aloft as was noted in the latter stages of the life cycle of C1.

The nature of the absolute angular momentum and kinetic energy budgets of the low troposphere was invariant between C1 and C2, namely, the buildup of absolute angular momentum in the low troposphere results from the excess of inward lateral transport over frictional torques and vertical export of absolute

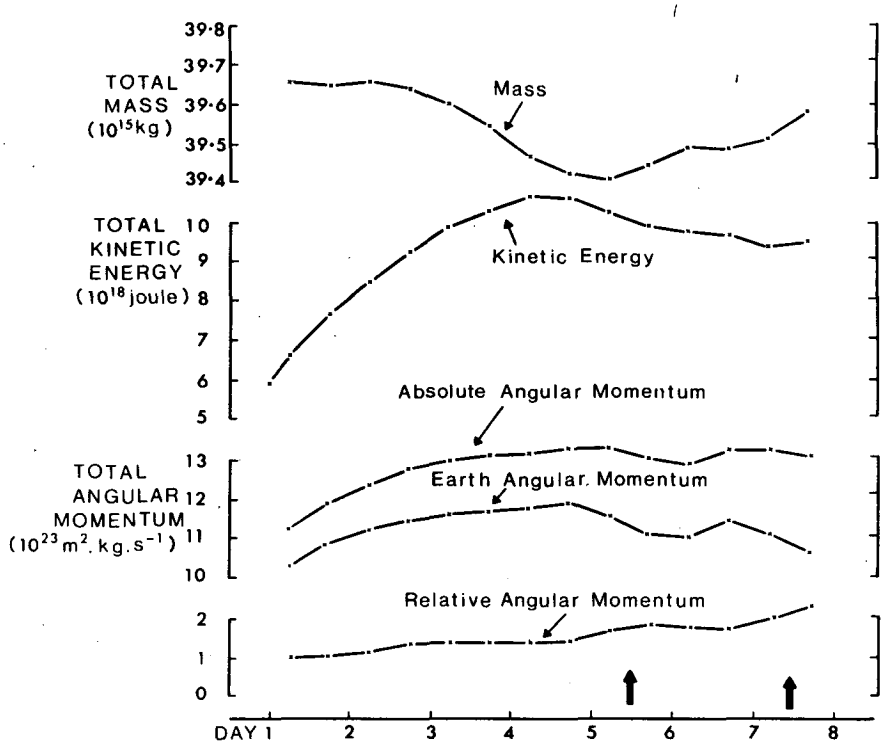

FIG. 12. Temporal distribution of the total mass, kinetic energy and angular momentum for cyclone C2. (Arrows on the time axis denote periods of fragmentation of surface center and/or secondary development.)

angular momentum. The mean mode of lateral transport is dominant in this process. The kinetic energy increase in the low troposphere which attends the angular momentum buildup is the result of local generation exceeding dissipation and vertical transport.

In the upper troposphere the early[5] buildup of angular momentum results from two effects: 1) vertical transport of angular momentum (this effect is generally largest in the early stages); and 2) the outward directed mean mode of absolute angular momentum associated with the mean mass circulation is offset by an inward directed eddy mode. This inward eddy mode results from the initial configuration of the upper flow (particularly jet streaks) and the mutual adjustments of the mass and momentum fields to the rotational deformation of the low and midtropospheric baroclinic zones which attend the low-level buildup of angular momentum.

The component terms of the total kinetic energy budget for C2 are shown in Fig. 13a (in contrast to Fig. 10a where lateral *export* and *dissipation* are plotted on the positive ordinate). A major feature is that throughout the entire life cycle of C2 there is positive generation and export of kinetic energy. In the early stages, the generation exceeds the export and dissipation to provide a positive tendency, while in the latter stages the situation is reversed. Fig. 13b shows the kinetic energy distribution for C2 at levels 3, 5 and 8. Another feature here is that although the kinetic energy is concentrated in the upper levels, the magnitude of the kinetic energy tendency in the lower and upper levels is quite comparable. This is in contrast to C1 where the tendency at the upper levels generally dominated. It is also significant that the tendency at level 3 for C2 is very different from the monotonic decrease we noted for C1. Since (topographical influences aside) surface cyclogenesis can be attended by energetically different configurations of the larger scale upper flow, it is unlikely that the tendency of the total kinetic energy budget in the immediate vicinity of extratropical cyclones can be uniquely related to their development or decay. Recent observational studies by Vincent and Chang (1975), Ward and Smith (1976) and others have shown the dominance of the upper levels in the overall kinetic energy budget and considerable variation in the role of the various terms with the type of synoptic regime being examined.

c. The anticyclone

Since in several respects the results for the anticyclone show inverse similarity to the cyclone, only a brief statement of the model features and budget results for the anticyclone is presented.

[5] As noted with C1, the reversal of the mass circulation aloft during the declining phase of the surface cyclone, can contribute substantially to the spin up of the upper troposphere in those latter stages.

The anticyclone considered is that shown south of New Zealand in the middle panel of Fig. 11a. In a synoptic sense the main features noted were that the central pressure and area-averaged pressure changed by relatively small amounts throughout the 6-day period of study and indeed a general feature of this model is its inability to produce anticyclones of comparable intensities to those found in the real atmosphere (this aspect is discussed in the next section) In the upper troposphere (500–200 mb) enhanced ridging appeared to be concurrent with the surface development.

As might be expected the profiles of the lateral mass transport showed a maximum convergence around 200 mb and maximum divergence in the surface boundary layer. In the upper troposphere an outward directed eddy mode of lateral transport and a downward vertical transport of absolute angular momentum resulted in a negative absolute angular momentum trend for the first 3 days. However, unlike the cyclone, the eddy mode does not appear to be enhanced by any frontogenetical effects in the lower troposphere and on the fourth day is outweighed by the inward mean mode.

The kinetic energy budget was dominated by the generation term in the upper troposphere. In the first few days this was large and positive and exceeded dissipation and export, only to be followed by a period of rapid decline before again reverting to large positive values. The energy budget of the upper troposphere was thereby different again from both of the cyclones. In contrast, the boundary layer of all three systems was characterized by a dominance of the generation and dissipation terms which to a first approximation balanced each other.

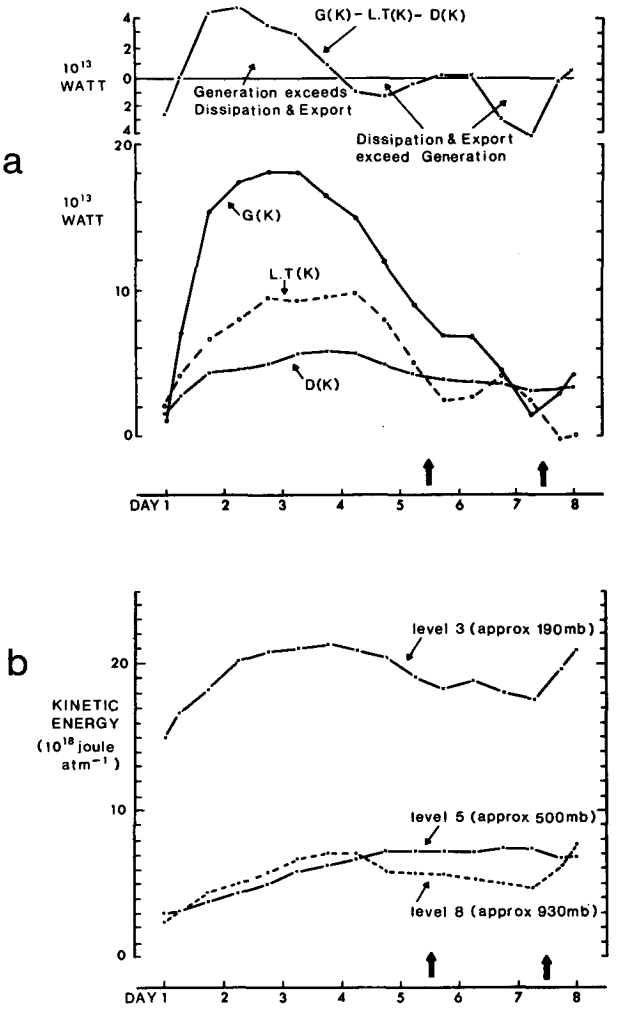

FIG. 13. Temporal distribution of (a) the component terms of the total kinetic energy budget (lower portion of figure) and their sum (upper) and (b) the kinetic energy at three selected levels, for cyclone C2. The area of the budget volume defined by a radius of 10° latitude is $\sim 0.39 \times 10^{13}$ m^2.

6. Conclusions and suggestions for future research

The results of the case studies we have examined suggested the following aspects are characteristic features of cyclogenesis in the model:

1) The lateral mass transport is dominated by effects in the boundary layer and at a level around 200 mb.

2) Mass convergence in the boundary layer facilitates spin up of the low troposphere in that the associated lateral transport of absolute angular momentum by the mean mode exceeds the opposing influence of frictional torques and vertical transport.

Since the outward mean mass circulation in the upper regions will remove absolute angular momentum, the buildup of absolute angular momentum in the upper troposphere must result from the influences of vertical transport and/or an eddy mode of lateral transport. The results show that both these effects are important. The lateral eddy mode is related to the configuration of the upper level flow and the adjustments to the rotational deformation and enhancement of the baroclinic zone in the lower/middle troposphere as the lower troposphere spins up. Sustained low-level development and the associated vertical and eddy lateral transports in the upper troposphere inevitably lead to the vertical collinearity of the upper trough and low-level vortex which typifies the occlusion phase of the cyclone.

The kinetic energy budget of the low troposphere is another characteristic feature. The increase in kinetic energy attending the low-level cyclogenesis is the result of local generation and lateral import exceeding the effects of dissipation and vertical export of kinetic energy. The dominant terms are the generation and dissipation.

The major variant feature noted in these studies is the kinetic energy budget of the upper troposphere. One can, of course, argue that this may in part be due to the fact that the geometry only encompasses a part

of the larger scale upper wave. However, the fact that the initial configuration and response of this limited region of the upper level flow can be so different is itself significant. It should be remembered that the role of friction in the model is prescribed by mixing length theory. In particular, only horizontal dissipation is prescribed above level 7. While the resultant form of the kinetic energy dissipation of one maximum in the boundary layer and a second in the region of the upper tropospheric jet stream is in agreement with Kung's (1966) observational results, the magnitudes observed in the upper levels were much less than the boundary layer values, whereas Kung suggests they may be equally as large. However, again this effect will very likely be masked by our limited examination of the upper wave, and most of the dissipation in the upper levels may be occurring in regions some distance from that encompassed by the low tropospheric vortex. Looking to future models, it will be interesting to see how they accommodate the recent observational results of Kung and Baker (1975), Tsui and Kung (1977), Ward and Smith (1976) and Chen and Bosart (1977). These studies indicate that in some cases there is a sub (super) synoptic-scale *source* of kinetic energy in the upper troposphere that is equal in magnitude to the boundary layer dissipation.

While the anticyclone budgets display similar features to the cyclone budgets there is one particular feature which is worthy of separate discussion. In the absolute angular momentum budget we noted that the eddy mode in the upper levels was (as with the cyclone) of considerable importance. However, whereas in the cyclone, the eddy mode in the upper regions may be reinforced by the low-level frontogenesis attending the generally convergent wind field of the surface cyclone, any similar effect in the anticyclone will be less marked by virtue of the weaker and divergent nature of the low-level flow.

Since the net eddy mode is very important in determining the total angular momentum budget, this aspect may be important in explaining why in general the scale of anticyclones more closely approaches that of the larger scale upper wave. Since the degree of horizontal resolution will in large part determine the ability to capture these eddy modes, the aforementioned inability of this model to produce anticyclones of comparable intensity to those observed in the real atmosphere may be partially due to inadequate horizontal resolution.

There are naturally many aspects of the cyclogenesis problem that the diagnostic studies reported here do not answer. It is of value to examine some of these, particularly with a view to future work which might be undertaken in this area.

The most obvious aspect is that while we have ascertained the nature of the mass circulation and the way in which that mass circulation transports properties such as angular momentum and kinetic energy in certain regions of the cyclone we are unable at this stage to say what initially forces this mass circulation and what determines the extent of the attendant cyclonic development. A persistent theme in the literature in this regard is that the configuration of the upper level flow is an important factor [e.g., Bjerknes and Holmboe, 1944; Sutcliffe and Forsdyke, 1950). Petterssen (1955), to name a few]. Certainly, the importance of an eddy mode of lateral transport in the case studies reported here, and in Johnson and Downey (1975b, 1976), supports this argument.

The perspective of this eddy mode of lateral transport and internal redistribution processes is, as noted in Johnson and Downey (1975a,b), coordinate-dependent. For example, the vertical transport term in sigma coordinates corresponds to three components of vertical redistribution in isentropic coordinates. One of these is directly related to diabatic effects and, in particular, to latent heat release. Unfortunately, the detailed vertical structure of the moisture budget for this case study was not readily available from the history tapes. An effort to enable retention of the three-dimensional distribution of moisture and latent heat release on these history tapes will have considerable priority in future studies.

A major test for any model is its short-term predictive capability and as noted in the Introduction there is a major application for the budget approach in this area. Here one might wish to examine the role of different initialization schemes, different horizontal and vertical resolutions, and different convective adjustment schemes on the mass, angular momentum and energetic adjustments occurring during cyclogenesis. Again where the model cyclogenesis compares favorably with the real atmosphere, the model with its internally consistent data base may provide the necessary insight into the problem. Where the models diverge from the real atmosphere, diagnosis of the latter may isolate the reasons.

Acknowledgments. A major part of this diagnostic work has involved a substantial computer programming effort. The authors are extremely grateful to Peter England and Les Logan of the Australian Numerical Meteorology Research Centre and Thomas Whittaker at the University of Wisconsin for their skillful accomplishments in this regard.

APPENDIX A

List of Symbols

F	budget integral
f	arbitrary budget quantity (per unit mass)
p	pressure
p_*	pressure at earth's surface
g	acceleration due to gravity
r	radius of the earth

$\mathbf{U}$	wind velocity
U_α	tangential component of $\mathbf{U}$
U_β	radial component of $\mathbf{U}$
$\mathbf{W}$	velocity of translating budget volume
$\dot{\mathbf{W}}$	acceleration of translating budget volume
R	gas constant
T	temperature
$\mathbf{F}$	friction
F_α	tangential component of $\mathbf{F}$
α	azimuthal coordinate
β	angular radial coordinate
β_B	value of β at boundary of budget volume
σ	vertical coordinate $[=p/p_*]$
$\dot{\sigma}$	$d\sigma/dt$
Ω	angular velocity of the earth
Φ	geopotential
ϕ	latitude
ϕ_0	latitude of center of budget volume
λ	longitude
λ_0	longitude of center of budget volume
$\Big\vert_{\beta_B}$	integral evaluated at boundary (where $\beta=\beta_B$)

APPENDIX B

Features of the Southern Hemisphere Version of the GFDL 9-level Stereographic Model

1) Climatological data used in the model (e.g., zonally averaged gaseous distributions, cloud cover, snowline) correspond to mean March conditions.

2) The convective adjustment scheme of Manabe, Smagorinsky and Strickler (1965) is adopted; however, the precipitation criterion used is a relative humidity of 80%.

3) The drag coefficient is constant over the whole hemisphere with a volume of 0.002.

4) Smoothed orography is included.

5) Limited land-sea contrast is included by using the heat balance equation only over land (the sea surface temperature remains fixed) and by employing a water availability factor of 0.5 over land. (Over the ocean it is set at 1.0.)

REFERENCES

Anderson, D. L. T., and P. Noar, 1974: The synoptic verisimilitude of a mid-latitude cyclone generated in a Southern Hemisphere general circulation model. *Mon. Wea. Rev.*, **102**, 613–629.

Bjerknes, J., 1937: Theorie der aussertropischen Zyklonenbildung. *Meteor Z.*, **54**, 462–466.

——, and J. Holmboe, 1944: On the theory of cyclones. *J. Meteor.*, **1**, 1–22.

Chen, T. J. G., and L. F. Bosart, 1977: Quasi-Lagrangian kinetic energy budgets of composite cyclone-anticyclone couplets. *J. Atmos. Sci.*, **34**, 451–465.

Johnson, D. R., and W. K. Downey, 1975a: Azimuthally averaged transport and budget equations for storms: Quasi-Lagrangian diagnostics I. *Mon. Wea. Rev.*, **103**, 967–979.

——, and ——, 1975b: The absolute angular momentum of storms: Quasi-Lagrangian diagnostics II. *Mon. Wea. Rev.*, **103**, 1063–1076.

——, and ——, 1976: The absolute angular momentum budget of an extratropical cyclone: Quasi-Lagrangian diagnostics III. *Mon. Wea. Rev.*, **104**, 3–14.

Kung, E. C., 1966: Large-scale balance of kinetic energy in the atmosphere. *Mon. Wea. Rev.*, **94**, 627–640.

——, and W. E. Baker, 1975: Energy transformations in middle-latitude disturbances. *Quart. J. Roy. Meteor. Soc.*, **101**, 793–815.

Manabe, S., J. Smagorinsky and R. F. Strickler, 1965: Simulated climatology of a general circulation model with a hydrologic cycle. *Mon. Wea. Rev.*, **93**, 769–798.

Petterssen, S., 1955: A general survey of factors influencing development at sea level. *J. Meteor.*, **12**, 36–42.

Simpson, R., and W. K. Downey, 1975: The effect of a warm mid-latitude sea surface temperature anomaly on a numerical simulation of the general circulation of the Southern Hemisphere. *Quart. J. Roy. Meteor. Soc.*, **101**, 847–867.

Smagorinsky, J., S. Manabe and J. Leith Holloway Jr., 1965: Numerical results from a nine-level general circulation model of the atmosphere. *Mon. Wea. Rev.*, **93**, 727–768.

Starr, V. P., 1953: Some aspects of the dynamics of cyclones. Geophys. Res. Pap. No. 24, MIT, 9–17.

Sutcliffe, R. C., and A. G. Forsdyke, 1950: The theory and use of upper air thickness patterns in forecasting. *Quart. J. Roy. Meteor. Soc.*, **76**, 189–217.

Tsui, T. L., and E. C. Kung, 1977: Subsynoptic-scale energy transformation in various severe storm situations. *J. Atmos. Sci.*, **34**, 98–110.

Vincent, D. G., and J. N. Chang, 1975: Kinetic energy budgets of moving systems: Case studies for an extratropical cyclone and hurricane Celia, 1970. *Tellus*, **27**, 215–233.

Ward, J. H., and P. J. Smith, 1976: A kinetic energy budget over North America during a period of short synoptic wave development. *Mon. Wea. Rev.*, **104**, 836–848.